The effects of an opposing buoyancy force on the performance of an air curtain in the doorway of a building

D. Frank, P. F. Linden

Department of Applied Mathematics and Theoretical Physics, University of Cambridge, Wilberforce Road, CB3 0WA Cambridge, United Kingdom

Abstract

We investigate the effects of an opposing buoyancy force on the performance of an air curtain in the doorway which separates a warm indoor environment from the cold exterior. Such an opposing buoyancy force arises for example if a downwards blowing air curtain is heated. We conducted small-scale experiments using water, salt and sugar solutions as the working fluids. The effectiveness curve of a downwards blowing air curtain as a function of the deflection modulus was measured for situations in which the initial density of the air curtain was less than both the indoor and the outdoor fluid density, which corresponds to the case of a heated curtain. It was found that the effectiveness of the air curtain starts to decrease if it is heated beyond a critical temperature. We also discuss the question whether it is more energy efficient to use a heated air curtain or an air curtain operating at room temperature. Based on our experimental results we conclude that a heated air curtain is likely to be less energy-efficient. Further, we propose a theoretical model to describe the dynamics of the buoyant air curtain. Numerical results obtained from solving this model corroborate our experimental findings.

Keywords:
air curtains, planar fountains, heat transfer

1. Introduction

Air curtains are commonly used as virtual barriers in doorways separating two different environments. Examples include public buildings with high human traffic such as shops or hotels, cold stores, industrial premises and hospitals. An air curtain can considerably reduce the mass, heat, moisture or particle exchange between two adjacent spaces without impeding the traffic through the doorway.

The design of air curtains is as versatile as the installation sites at which they are deployed [1]. An air curtain can be directed either vertically or horizontally, it can consist of one or multiple jets, the primary air supply may be drawn from inside or outside or even additionally heated or cooled, and the air curtain may be inclined or designed as a recirculatory system with a return grill at the opposite side of the door frame. However, regardless of the specific details, the basic operating principle of air curtains is always the same. A high-velocity plane jet is discharged from a thin nozzle located on one side of the door frame. The planar jet is usually subjected to transversal forces which are most commonly due to either the stack effect resulting from a temperature difference across the doorway or the wind pressure. As the jet travels across the opening, it entrains fluid from both sides of the doorway, mixes it to a certain degree and then spills the fluid back again when it impinges on the opposite site of the doorframe. This process is commonly known as the entrainment-spill mechanism of the air curtain [2, 3].

The basic idea of the aerodynamical sealing dates back to the beginning of the 20th century [2, 4]. However, air curtains grew in popularity only in the last 50 years with the raising awareness for thermal comfort, energy saving and, more recently, climate change. The first systematic studies on the sealing ability of air curtains were carried out in 1960s. Based on full-scale experimental results, Hayes and Stoecker [2, 5] presented a fundamental discussion of the air curtain stability. An air curtain is called stable if it reaches the opposite side of the doorway and impinges on it. In contrast, the air curtain is said to be unstable and to break through if it is deflected too much out of the plane of the door frame by the lateral pressure difference until it discharges hor-

Email address: D.Frank@damtp.cam.ac.uk (D. Frank)

Nomenclature

$\triangle$	reduced gravity acceleration $\triangle = g(\rho_l/\rho - 1)$
b	width of the jet [m]
C_d	discharge coefficient
D_m	deflection modulus
ds	variation along the streamline coordinate
dx	variation along the horizontal direction
dz	variation along the vertical direction
E	effectiveness of the air curtain
g	gravitational acceleration [m/s^2]
g'	reduced gravity acceleration $g' = g(1 - \gamma)$ [m/s^2]
H	height [m]
h	height [m]
L_j	jet length [m]
m	momentum flux per unit length [m^3/s^2]
q	volume flow rate through the (unprotected) door [m^3/s]
q_a	volume flow rate through the door with an operating air curtain [m^3/s]
Re	Reynolds number
T	temperature [K]
t	time [s]
u	centreline velocity [m/s]
V	volume of the enclosure [m^3]
V_{meas}	experimentally measured volume of dense fluid intruding the light fluid half [m^3/s]
w	width [m]
x	coordinate into horizontal direction
z	coordinate into vertical direction

Greek letters

α	inclination angle of the jet to the vertical
α_E	entrainment constant
β	density ratio ρ_0/ρ_l
ϵ	fraction of the initial volume flux through the air curtain spilled back to the light fluid side of the doorway
γ	density ratio ρ_l/ρ_d
Λ	energy efficiency
ν	kinematic viscosity [m^2/s]
ρ	(total) density [kg/m^3]
$\tilde{\Lambda}$	modified energy efficiency
$\tilde{\rho}$	density associated with the addition of salt alone [kg/m^3]

Subscripts

0	value at the nozzle or start-up time t_0
$\star$	apparent effectiveness $E_\star$ or lower bound on energy efficiency $\Lambda_\star$
b	bottom opening, i.e., doorway
d	dense fluid
l	light fluid
min	minimum
w	water
x	horizontal coordinate direction
z	vertical coordinate direction

Superscripts

new	at the end of the experimental run

izontally to one side of the doorway and leaves part of the door opening unprotected. Hayes and Stoecker [2] identified the deflection modulus D_m, which is the ratio between the air curtain momentum flux at the outlet and the transversal forces acting on it, as the main parameter governing the air curtain dynamics and formulated the stability criterion in terms of the minimum deflection modulus $D_{m,min}$. Furthermore, Hayes and Stoecker predicted numerically the heat transfer due to the entrainment-spill mechanism of the air curtain. The fraction by which the heat transfer with an operating air curtain is reduced compared to the open-door situation is called the effectiveness of the air curtain.

Since then, various theoretical, numerical and experimental studies have been conducted to investigate the air curtain stability and the heat transfer associated with it. Howell and Shibata [6] carried out full-scale experiments for a recirculated plane air curtain with a re-

turn grill and confirmed theoretical predictions of [2]. For this investigation they used a downwards blowing chilled air curtain so that the additional buoyancy force was assisting the jet flow.

The experimental field study on the sealing ability of a commercial air curtain for refrigerated chambers was conducted in [7]. In particular, Foster et al. measured the effectiveness curve of the air curtain as a function of its discharge velocity and concluded that leakage around the air curtain edges could have an impact on its performance. The inner structure of the air curtain and its use as a smoke barrier in tunnels was examined in [8]. There are also multiple numerical studies on the air curtain performance, such as reported in [7, 9, 10, 11] as well as semi-analytical models to assess the heat transfer associated with air curtains [12].

A detailed theoretical study of the technical air curtain dimensioning was presented by Sirén in [1, 3]. Sirén investigated the stability of the air curtain under presence of additional wind pressure term and also included effects of leakage distribution into the discussion.

The effects of a leakage distribution in the building envelope and of an additional ventilation opening on the air curtain performance was further investigated in [13]. It was found that the air curtain can operate in four different operating regimes depending on the deflection modulus value and the enclosure geometry. In particular, for relatively small values of D_m the flow through the room is driven by the flux through the ventilation opening whereas for large values of D_m the flow is controlled by the air curtain flow with a smooth transition occurring between these two regimes. In [13], theoretical estimates were presented for the air curtain performance in the case of a ventilated enclosure. They showed a good agreement with experimental results which were obtained in the same study using a small-scale experimental setup and water as the working fluid.

Despite this previous research on air curtains, one factor has been neglected in the discussion of the air curtain performance and stability. If a downwards blowing air curtain is heated (or equivalently, an upwards blowing air curtain is cooled), then there is an additional buoyancy force acting against the jet flow direction. In this case, the air curtain is no longer a simple planar jet but is classified as a line source fountain [14]. One question in this context is for which range of parameters this additional buoyancy force can be neglected, and when it starts to modify the air curtain dynamics so that the stability criterion as formulated by Hayes and Stoecker [2] is no longer valid. Furthermore, it is also of importance to know whether and how the additional buoyancy force modifies the heat and mass transfer characteristics between two environments. Although heated air curtains are commonly installed in doorways with pedestrian traffic, there seem to be no systematic studies on the behaviour of a buoyant air curtain.

In this paper, we address this question of the performance of a buoyant air curtain. First, we define the basic quantities describing the air curtain and the turbulent fountain dynamics. Then we discuss small-scale experiments for a model enclosure with an air curtain which were conducted using water as working fluid with salt and sugar as tracers, and present the results for the sealing effectiveness of a buoyant air curtain. Subsequently, we set up a system of differential equations governing the air curtain dynamics and solve it numerically. The numerical results for the air curtain stability are compared to the experimental data and good agreement is found. We conclude this paper with a discussion of an application of our results to a real building.

2. Theoretical background

In the following, we consider the configuration of the enclosure as presented in Fig. 1. The enclosure filled with fluid of density ρ_l and temperature T_l ("light") is connected to the ambient environment with fluid of density $\rho_d > \rho_l$ and temperature $T_d < T_l$ ("dense") by means of a doorway with height h_b and width w_b. We consider an air curtain which is fitted to the upper edge of the doorway and discharged downwards with velocity u_0 from a thin nozzle of width b_0. The initial air curtain density and temperature are denoted by ρ_0 and T_0, respectively, and we assume $\rho_0 < \rho_l$ so that the air curtain is buoyant with respect to the enclosure as well as with respect to the ambient. The density ratios $\gamma = \rho_l/\rho_d$ and $\beta = \rho_0/\rho_l$ shall be close to 1 as typical in practice, so that the Boussinesq approximation applies. The pressure distribution indoors and outdoors is assumed to be hydrostatic. Also, we ignore the effects of wind and assume that the pressure difference between indoors and outdoors is caused solely by the stack effect.

In the following, we restrict our attention to the following door-opening process: the door is opened instantly and the air curtain is switched on simultaneously. The door remains open for a certain time t. Subsequently, the door is closed instantly and the air curtain is switched off again. We assume that the exchange flow is steady during the door opening time t.

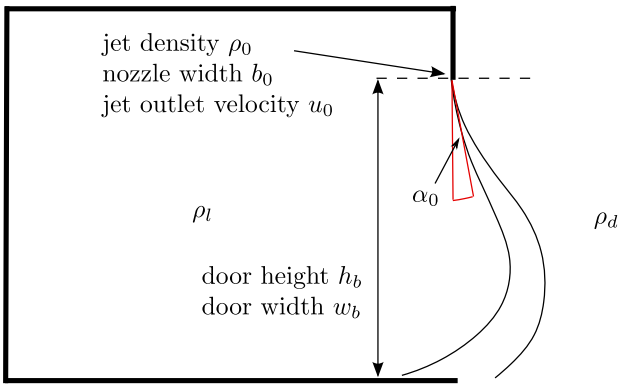

Figure 1: Geometry of the enclosure and the air curtain.

2.1. Minimum deflection modulus

According to [2, 5] the main parameter governing the air curtain behaviour is the deflection modulus:

$$D_m = \frac{\rho_0 b_0 u_0^2}{g h_b (\rho_d - \rho_l)} = \frac{b_0 u_0^2}{g h_b \left(\frac{T_0}{T_d} - \frac{T_0}{T_l}\right)} \tag{1}$$

where g is gravity. Using conservation of x-momentum in the fixed volume (shown in Fig. 8) it can be deduced (cf. [5, 1, 13]) that the air curtain is stable if

$$D_m \gtrapprox \frac{1}{8} \tag{2}$$

provided that the pressure difference is caused by the stack effect. Hayes and Stoecker [5] included an additional pressure term into their discussion, the so called auxiliary pressure which is the self-made pressure of the air curtain. Thus, the minimum deflection modulus $D_{m,min}$ recovered by Hayes and Stoecker is slightly higher than given by Eq. (2). However, these results for $D_{m,min}$ are all on the boundary of stability so that for a real air curtain a safety factor between 1.3 and 2 should be applied [2, 7].

The effect of the vertical leakage distribution in the building envelope on the minimum deflection modulus $D_{m,min}$ was investigated in [1] and in [13]. It was found in [13] that $D_{m,min}$ rises significantly once the building envelope is no longer tight or if there is an additional ventilation opening.

One of the questions which we address in this paper is whether the value of $D_{m,min}$ is affected by the additional buoyancy force acting on the heated air curtain.

2.2. Effectiveness

The effectiveness E of the air curtain is defined as the fraction of the flow, which is prevented by the air curtain compared to the open-door situation:

$$E = 1 - \frac{q_a}{q} \tag{3}$$

where we denote by q_a the volume flow rate of ambient fluid into the enclosure when the air curtain is working and by q the corresponding inflow for an unprotected opening. For a single opening, the inflow rate q is calculated using the orifice equation:

$$q = C_d \frac{w_b h_b}{3} \sqrt{g' h_b} \tag{4}$$

where $g' = g(1 - \gamma)$ is the reduced gravity. The experimentally measured discharge coefficient C_d has a value of around 0.6 for sharp-edged openings [15, 16].

2.3. Jet length

The presence of an opposing buoyancy force implies that a heated downwards blowing air curtain is no longer a planar turbulent jet but rather a turbulent line source fountain. The fountain behaviour differs from the jet behaviour insofar as the fountain continues to intrude into the ambient fluid only up to a well defined distance which depends on the initial momentum flux and buoyancy flux of the fountain. At this distance, the initial momentum flux of the fountain is counterbalanced by the work done by the opposing buoyancy force and, hence, at this distance the flow in the fountain is reversed. In order to quantify the buoyancy intensity of the air curtain, we introduce the jet length:

$$L_j = \frac{m_0}{(u_0 b_0 \triangle_0)^{2/3}} \tag{5}$$

which is a combination between the momentum flux per unit length $m_0 = b_0 u_0^2$ and buoyancy flux $b_0 u_0 \triangle_0$ per unit length at the outlet where we define $\triangle_0 = g\,(\rho_l/\rho_0 - 1)$.

2.4. Apparent effectiveness

The effectiveness E of the air curtain is defined in terms of the ambient fluid flow intruding the enclosure with and without the air curtain. In other words, if the ambient fluid was dyed, the effectiveness E would indicate by how much the change in the dye concentration inside the enclosure is reduced if the air curtain is operating compared to the open-door situation. However, since the primary air curtain flow q_0 is heated, the temperature change inside the room is not solely determined by the ambient fluid inflow. In fact, depending on the heating strength of the primary air curtain flow q_0, the temperature inside the enclosure may either decrease,

remain the same or even rise during the previously described door-opening cycle with an operating air curtain. In order to account for this temperature change inside the enclosure we define the apparent effectiveness as:

$$E_\star = 1 - \frac{\triangle\rho\big|_{air-curtain}}{\triangle\rho\big|_{open-door}} = 1 - \frac{\left(\rho_l^{new} - \rho_l\right)\big|_{air-curtain}}{\left(\rho_l^{new} - \rho_l\right)\big|_{open-door}} \quad (6)$$

Thereby, we denote by ρ_l^{new} the average fluid density in the enclosure at the end of the door-opening cycle when the door is closed again.

We have $E_\star < 1$ if the temperature in the room is decreased during the door-opening cycle and $E_\star = 1$ if the temperature does not change. The case $E_\star > 1$, when the temperature in the room is increased, is impossible in the unheated case for which $\rho_0 = \rho_l$. This case occurs when the primary flow q_0 of the air curtain is so strongly heated that, even after the turbulent mixing with the ambient fluid, the fluid which is spilled back to the cavity has a higher temperature than the room temperature.

Note that the definition of $E_\star$ is independent of the door-opening time t if we assume a steady fluid exchange between the indoor environment and the ambient. This can be seen as follows. The fluid density in the enclosure at the end of the door-opening cycle with an operating air curtain can be calculated as:

$$\begin{aligned}\rho_l^{new}\big|_{air-curtain} &= \frac{\rho_l\left(V - q_a t - \epsilon q_0 t\right) + \rho_d q_a t + \rho_0 \epsilon q_0 t}{V} \\ &= \rho_l + (\rho_d - \rho_l)\,\frac{q_a t}{V} + (\rho_0 - \rho_l)\,\frac{\epsilon q_0 t}{V}\end{aligned} \quad (7)$$

where V is the volume of the enclosure and ϵ is the fraction of the initial volume flux through the air curtain at the nozzle which is spilled back to the enclosure when the air curtain impinges on the floor. Note that we implicitly make an incompressibility assumption here and hence use volume conservation for the interior of the room. In a similar way we can calculate the fluid density in the room at the end of the door-opening cycle when the air curtain is switched off:

$$\rho_l^{new}\big|_{open-door} = \frac{\rho_l\left(V - qt\right) + \rho_d qt}{V} = \rho_l + (\rho_d - \rho_l)\,\frac{qt}{V} \quad (8)$$

Inserting Eqs. (7) and (8) into Eq. (6) shows that the definition of $E_\star$ does not depend on t.

Furthermore, in case of a neutrally buoyant air curtain for which $\rho_0 = \rho_l$ the last term of Eq. (7) vanishes so that Eq. (6) reduces to Eq. (3). Thus, for a neutrally buoyant air curtain we have:

$$E_\star = E \quad (9)$$

3. Experimental setup

In order to investigate the performance of a buoyant air curtain, we performed small-scale experiments using fresh water and salt and sugar solutions as working fluids. We used the same experimental setup as reported in [13]. It consisted of a tank with dimensions 0.58 m × 0.58 m × 0.59 m and a separation barrier in the middle (Fig. 2). The separation barrier had a door opening of width $w_b = 0.1$ m. The height h_b of the door opening could be varied up to 0.3 m by means of a removable sluice gate. An air curtain device (ACD) was fitted just above the top edge of the door opening in one half of the tank. The ACD consisted of a horizontal circular tube with an adjustable thin slit nozzle of width b_0 on its lower side. The original length of the air curtain tube was 0.2 m and both ends of the device were sealed with an adhesive foil so that the air curtain length matched the door width w_b. The water to the air curtain was provided from a separate constant head tank placed above the experimental tank which guaranteed a steady flow rate through the air curtain. The flow rate was monitored using the flow meter FLR1013 manufactured by Omega with the accuracy ±3% FS.

During the experiments on the sealing behaviour of a buoyant air curtain we fixed the nozzle width of the air curtain to $b_0 = 0.001$ m. The doorheight h_b was set during first few experiments to $h_b = 0.125$ m but then readjusted to $h_b = 0.2$ m in order to achieve lower values of L_j/h_b. The ACD was located on the light fluid side of the tank which corresponds to the case of a real air curtain being placed inside the warm room. The primary water supply to the air curtain device was fresh water of density ρ_0. The initial flow rate through the air curtain was about $q_0 = 4.2$ l/min during this series of experiments.

The experimental procedure consisted of the following steps. One half of the tank was filled with salt water of density ρ_d up to the height of $H_w = 0.3$ m and the other half of the tank was filled with sugar solution of density ρ_l up to the same height $H_w = 0.3$ m. The density difference $\triangle\rho = \rho_d - \rho_l$ between two halves of the tank could be varied so that the values of the deflection modulus D_m in the range 0.2 - 0.8 were achieved. Higher values of the deflection modulus were not possible since the change in the density in the light (sugar) fluid half of the tank at the end of the experimental run could not be measured precisely for very small initial density differences $\triangle\rho < 3 \cdot 10^{-3}$ g/cm^3.

The density of light (sugar) fluid ρ_l was chosen such that the ratio L_j/h_b was in the range 0.7 - ∞ where the limit $L_j/h_b \to \infty$ corresponds to the case of a neu-

trally buoyant air curtain with $\rho_0 = \rho_l$. For the given experimental configuration, the value $L_j/h_b = 0.7$ was achieved with the light fluid density of $\rho_l \approx 1.02\,\mathrm{g/cm^3}$. Note, in particular, that in our experiments we keep the density ρ_0 fixed since we supply the ACD with fresh water and vary the density ρ_l by adding sugar to achieve different values of L_j/h_b. In real buildings, the desired inside temperature T_l (i.e., the density ρ_l) is usually prescribed and it is the air curtain discharge temperature T_0 (i.e., the density ρ_0) which can be adjusted. Therefore, in the following we will use the notation $\rho_0 \to \rho_l$ when discussing the limiting case of the neutrally buoyant air curtain and not $\rho_l \to \rho_0$.

The densities ρ_l and ρ_d were measured using Anton-Paar density meter DMA 5000 with accuracy of $10^{-5}\mathrm{g/cm^3}$. Furthermore, the salt content in the light fluid half was determined using the conductivity probe which was calibrated using the aforementioned density meter. Since the light (sugar) water did not contain any salt initially, and sugar is non-conductive, the measured density $\tilde{\rho}_l$ of light fluid using the conductivity probe was the same as the fresh water density.

The experiment was started by switching on the air curtain device. We had to allow for a few seconds (typically 5 - 7 sec) to pass before the flow rate through the air curtain device reached a constant value. A correction in all the calculations was made to account for this time t_0 at the beginning of the experiment during which the air curtain was operating but the doorway was still closed. Once q_0 was constant, we opened the doorway and started the time measurement. The fluid was allowed to exchange between two halves of the tank for about $t = 30$ s. At the end of the experiment, the door was closed again and the air curtain device switched off.

Subsequently, the water was thoroughly mixed in both halves of the tank. The salt content in the light fluid half of the tank was again determined using the conductivity probe. We measured the new density $\tilde{\rho}_l^{new}$, associated with the salt alone, and using the difference $\tilde{\rho}_l^{new} - \tilde{\rho}_l$ we could calculate the amount of salt water intruding the light fluid half of the tank during the experiment. In addition, we also measured the new densities ρ_l^{new} and ρ_d^{new} (which included the contributions from both salt and sugar) using the density meter in order to calculate $E_\star$.

Note that our experiments were conducted with the free water surface and that the fluid was constantly added to the tank by the air curtain. However, this added amount of fluid was just a small fraction of the whole water volume in the tank (as argued later) so that it did not significantly alter the experimental conditions.

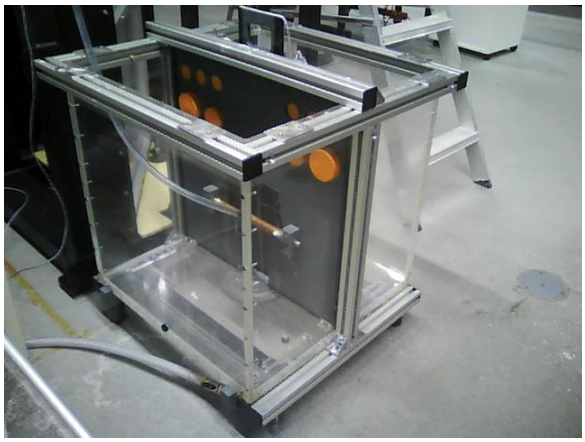

Figure 2: Experimental tank.

3.1. Dynamical similarity

The dynamical similarity between our small-scale experiments and full-scale real air curtain installations is ensured as was discussed in detail in the previous study [13]. The dynamical similarity relies on the nozzle-based Reynolds number $Re = u_0 b_0/\nu$, where ν is the kinematic viscosity. In our small-scale experiments we reduced the discharge velocity u_0 by the factor of 10 and kept the nozzle width in approximately the same range. Since $\nu_{air}/\nu_{water} \approx 10$, the Reynolds number in our small-scale experiments is of the same magnitude as for real air curtain installations.

3.2. Why are two tracers necessary?

As has been mentioned previously, the density change in the enclosure during the door-opening cycle is associated with two components: the intruding ambient fluid and the fraction ϵ of the primary air curtain flow q_0 which is spilled back to the enclosure. In order to properly measure the effectiveness E of the air curtain, it is necessary to differentiate between these two components. Therefore, we use salt and sugar as tracers in our experiments. In the following, we explain why the differentiation between two components in the density change is crucial and why just one tracer is insufficient for precise measurements.

In order to calculate the effectiveness E we need to know the volume of dense fluid V_{meas} which intrudes the light fluid half during an experimental run. This volume V_{meas} of dense fluid can be determined using the appropriate mass balance equation for the light fluid half of the tank.

If we use just one tracer, then the mass balance for

the light fluid half reads:

$$\rho_l^{new}\,(V + \epsilon q_0 t + 0.5 q_0 t_0) = \rho_l\,(V - V_{meas}) + \rho_d V_{meas} + \rho_0\,(\epsilon q_0 t + 0.5 q_0 t_0) \tag{10}$$

where V is the initial fluid volume in one half of the tank. The left-hand side of this equation is the total mass in the light fluid side of the tank at the end of the experiment. The right-hand side of this equation sums the various contributions to this total mass: the original light fluid which remains in the light-fluid half, the intruding amount of dense water and the fluid added due to the initial fluid flow through the air curtain, respectively. Note, that we include the correction $0.5 q_0 t_0$ to account for the starting-up time of the ACD. The factor 0.5 is reasonable if we assume that the flow rate through the air curtain varies linearly until it reaches a constant value at the time t_0. As before, we denote by ϵ the part of the initial air curtain flow which is spilled back to the enclosure, i. e., the light fluid half of the tank.

Equation (10) can be rearranged to calculate V_{meas}:

$$\frac{V_{meas}}{V} = \frac{\rho_l^{new} - \rho_l}{\rho_d - \rho_l} + \frac{\rho_l^{new} - \rho_0}{\rho_d - \rho_l}\,\frac{\epsilon q_0 t + 0.5 q_0 t_0}{V} \tag{11}$$

The exact value of ϵ is a priori not known. Since the air curtain device is located in the light fluid half of the tank, we can expect ϵ to be in the range 0.5 - 1. For the used running times of about 30 seconds, the initial flow rate through the air curtain of 4 l/min and the initial water volume in the light fluid half of the tank of about 50 l, the corresponding correction $\epsilon q_0 t/V$ is about 4% if ϵ is assumed to be 1 and only 2% if ϵ is set to 0.5. This also implies that the correction $0.5 q_0 t_0/V$ is small as well. However, in the experimental runs with a strongly buoyant air curtain, we have $\rho_l - \rho_0 \gg \rho_d - \rho_l$ and, since the change in the density in the light-fluid half $\rho_l^{new} - \rho_l$ is observed to be relatively small, we also have $\rho_l^{new} - \rho_0 \gg \rho_d - \rho_l$. Thus, in this case, the second term in Eq. (11) is in the same order of magnitude as the first one and the exact unknown value of ϵ has a strong impact on the calculated value of V_{meas}.

In contrast, if we use two tracers in our experiments as specified above we can distinguish between two components associated with the density change in the enclosure. In that case, salt is contained only in the dense fluid half of the tank and not in the primary air curtain flow q_0. We can set up the following mass balance for salt:

$$(\tilde{\rho}_l^{new} - \tilde{\rho}_l)\,(V + \epsilon q_0 t + 0.5 q_0 t_0) = V_{meas}\,(\rho_d - \tilde{\rho}_l) \tag{12}$$

The left-hand side of this equation is the mass of salt measured in the light fluid half at the end of the experiment whereas the right-hand side is the mass of salt which is added to the light fluid half due to the fluid inflow from the salt water half. We can express V_{meas} as:

$$\frac{V_{meas}}{V} = \frac{\tilde{\rho}_l^{new} - \tilde{\rho}_l}{\rho_d - \tilde{\rho}_l}\left(1 + \frac{0.5 q_0 t_0}{V} + \frac{\epsilon q_0 t}{V}\right) \tag{13}$$

Now, as argued above the correction $\epsilon q_0 t/V$ is small and we can assume the unknown quantitity ϵ to have any value between 0.5 and 1 without introducing an error of more than 1%. Since the error in V_{meas} due to the measurement of the involved densities, flow rate and time amounts to a few percent (usually between 2% and 5%), this uncertainty due to the unknown parameter ϵ does not increase the total error significantly. This discussion shows that we indeed need two tracers for precise measurement of V_{meas} and E.

4. Experimental results

4.1. Effectiveness E of the buoyant air curtain

This subsection describes the experimentally obtained results for the air curtain effectiveness E.

In order to determine the effectiveness of the buoyant air curtain, we calculate the intruding volume by Eq. (13). The reference intruding volume of salt water into the light fluid half without the air curtain is computed using the orifice equation Eq. (4) with the discharge coefficient $C_d = 0.57$, the measurement of which we reported in [13].

We show the measured effectiveness values depending on D_m for different values of L_j/h_b in Fig. 3. Note that it is almost impossible to ensure the exact same value of L_j/h_b for two consecutive experiments. Therefore, the curves shown in Fig. 3 comprise the measured data for approximately the same values of L_j/h_b. For example, for the curve indicated with "$L_j/h_b = 1.14$" the actual values of L_j/h_b vary between 1.13 and 1.15, and this amount of variation is typical.

From Fig. 3 we observe the following behaviour of the buoyant air curtain effectiveness. For large values of L_j/h_b (e.g., $L_j/h_b \gtrsim 2$) the additional buoyancy force does not affect the performance of the air curtain. We recover essentially the same effectiveness curve as in the isothermal case $\rho_0 = \rho_l$ which was obtained using the same experimental setup in [13]. Here, the air curtain impinges on the bottom of the doorway and still provides a good aerodynamical sealing. The schematic

of the impinging air curtain is shown in Fig. 4a. For values of $L_j/h_b \lesssim 1.14$ we begin to observe the decrease in the air curtain effectiveness. In this case the fountain behaviour of the air curtain becomes important: the flow through the air curtain is reversed before the air curtain can properly impinge on the bottom of the doorway. The air curtain does not effectively cover the opening in the vicinity of the bottom so that a leakge might occur in this region, Fig. 4b. For the value of $L_j/h_b = 1.14$ the effectiveness is reduced by 15 - 20% in the range of the D_m values of 0.2 - 0.5 compared to the isothermal case. The effectiveness is further reduced for smaller values of L_j/h_b, so that for $L_j/h_b = 0.92$ we recover $E \approx 0.5$ for $D_m \in [0.2, 0.5]$ (for the isothermal air curtain the effectiveness values are around 0.8 - 0.9 in this D_m parameter range). Furthermore, it appears that for a buoyant air curtain the D_m value for which the effectiveness is at its maximum is shifted to higher values of the deflection modulus. For example, for an isothermal air curtain, the maximum effectiveness is attained for $D_m \approx 0.35$, for $L_j/h_b \approx 1.14$ the maximum effectiveness is reached for $D_m \approx 0.55$ and for $L_j/h_b \approx 0.92$ it is reached for $D_m \approx 0.65$.

4.2. Apparent effectiveness $E_\star$ of the buoyant air curtain

We now determine the apparent effectiveness $E_\star$ in our experiments. In the case of the non-heated air curtain, the apparent effectiveness $E_\star$ coincides with the effectiveness E as has already been shown.

Figure 5 shows the apparent effectiveness which we measured in our experiments. Blue dots indicate the experimental runs in which the room was colder at the end of the experiment ($\rho_l^{new} > \rho_l$), i.e., $E_\star < 1$ and red triangles depict the cases in which the room was warmer at the end of the experiment ($\rho_l^{new} < \rho_l$), i.e., $E_\star > 1$. The case $E_\star > 1$ occurs if the air curtain is so strongly heated that even after the turbulent mixing with the ambient fluid, the fluid spilled back to the enclosure is of higher temperature (smaller density) than the fluid inside the room. For each value of D_m we can expect a unique value of L_j/h_b for which we have $E_\star = 1$, which means that L_j/h_b (i.e., discharge velocity u_0 and the initial jet density ρ_0) is exactly adjusted so that the room temperature does not change during the experiment.

4.3. Energy efficiency: comparison between an isothermal and a heated air curtain

In the discussion of a buoyant air curtain, one question inevitably arises regarding the energy efficiency of the heated air curtain versus the isothermal air curtain. From the energetic point of view, is it better to use a heated air curtain and adjust its momentum flux and buoyancy so that the apparent effectiveness is $E_\star = 1$ (i.e., fluid added to the enclosure by the air curtain attains the room temperature) or is it more energy-saving to install a neutrally buoyant air curtain with $\rho_0 = \rho_l$ and subsequently to heat up the intruding ambient fluid until it reaches the room temperature? In order to examine this problem, we define the energy efficiency:

$$\Lambda = \frac{q_0\big|_{buoyant}(\rho_l - \rho_0)}{q_a\big|_{isothermal}(\rho_d - \rho_l)} = \frac{q_0\big|_{buoyant}\left(1 - \frac{1}{\beta}\right)}{q_a\big|_{isothermal}\left(\frac{1}{\gamma} - 1\right)} \quad (14)$$

This quantity describes the ratio between two energy rates: the energy rate needed to heat up a buoyant air curtain from the room temperature to its discharge temperature, and that needed to heat up the intruding flux of the dense fluid to the room temperature for the isothermal air curtain. We denote by $q_0\big|_{buoyant}$ the primary air flow through the buoyant air curtain. Moreover, $q_a\big|_{isothermal}$ is the intruding flux of the dense ambient fluid into the enclosure due to the turbulent mixing in the reference case when a neutrally buoyant air curtain with $\rho_0 = \rho_l$, and with otherwise the same parameters (i.e., the same nozzle width b_0 and the same outlet velocity u_0), is used. A priori, $q_a\big|_{isothermal}$ is an unknown quantity for a given deflection modulus and geometry of the opening. It can be experimentally deduced by a meticulous measurement of the effectiveness curve of the isothermal air curtain. However, we will see shortly how this difficulty can be otherwise avoided.

The energy efficiency Λ can be calculated for arbitrary values of $q_0\big|_{buoyant}$ and β, but it is primarily important for the case in which for a given deflection modulus D_m, the ratio L_j/h_b (and, hence, $q_0\big|_{buoyant}$ and β) is adjusted so that $E_\star = 1$. If for $E_\star = 1$, we have $\Lambda < 1$, then it is more energy-saving to heat the air curtain. The other case $\Lambda > 1$ implies that from the energetic point of view it is better to use an isothermal air curtain.

The energy efficiency Λ as defined by Eq. (14) requires the knowledge of the reference flux $q_a\big|_{isothermal}$ which is the intruding flux of the dense fluid into the enclosure if the isothermal air curtain is used. However, recalling the experimental result that the effectiveness E decreases with decreasing L_j/h_b from previous section, we argue that $q_a\big|_{isothermal} \leq q_a\big|_{buoyant}$ and, thus:

$$\Lambda = \frac{q_0\big|_{buoyant}(\rho_l - \rho_0)}{q_a\big|_{isothermal}(\rho_d - \rho_l)} \geq \frac{q_0\big|_{buoyant}(\rho_l - \rho_0)}{q_a\big|_{buoyant}(\rho_d - \rho_l)} =: \Lambda_\star \quad (15)$$

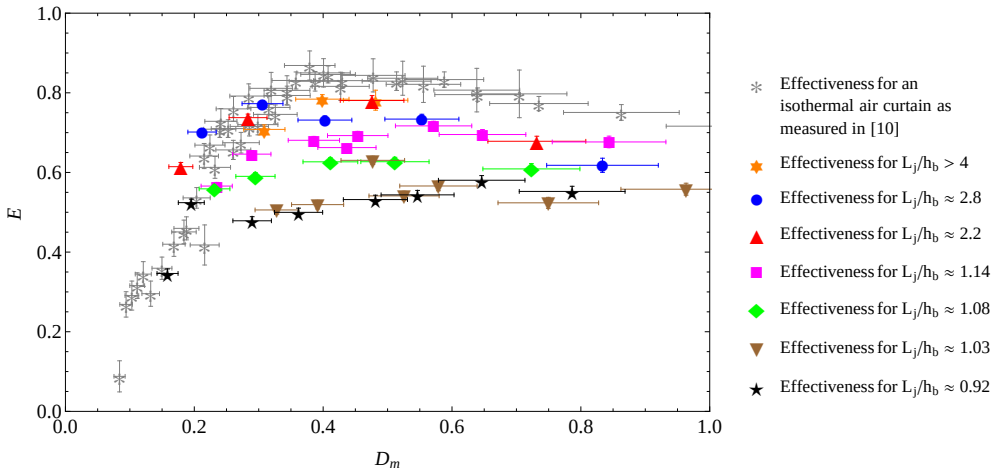

Figure 3: Experimentally measured effectiveness E of the air curtain for different values of L_j/h_b.

Figure 4: Possible operating regimes for the buoyant air curtain: (a) a weakly heated air curtain which impinges on the bottom of the doorway, (b) a strongly heated air curtain with a dominant fountain behaviour so that the flow is reversed before the air curtain can impinge on the bottom of the doorway.

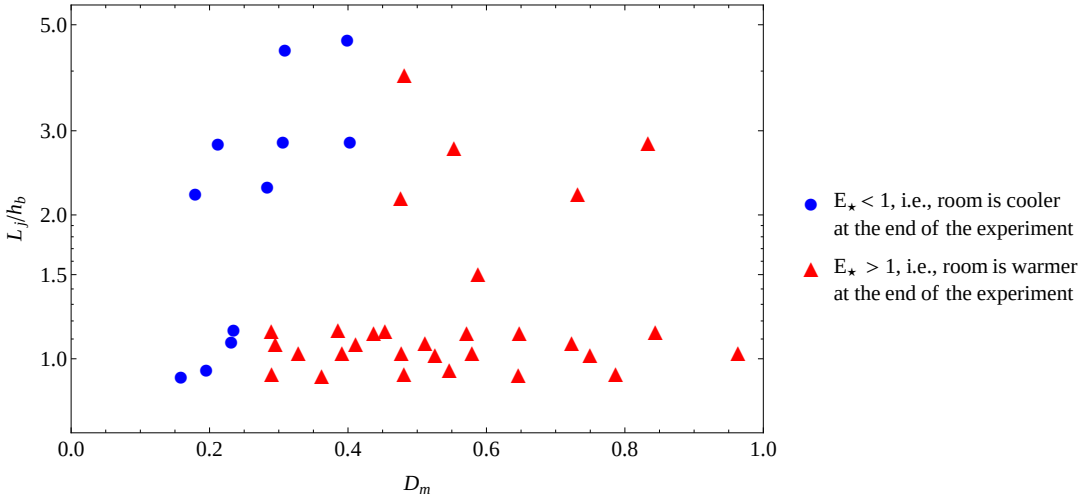

Figure 5: Experimentally measured apparent effectiveness of the buoyant air curtain.

Thereby, $q_a\big|_{buoyant}$ is the intruding flux of dense fluid into the cavity when the heated air curtain is switched on. Hence, the lower bound $\Lambda_\star$ for the energy efficiency Λ can be calculated directly for each experimental measurement of the buoyant air curtain. For $L_j/h_b \to \infty$, i.e., for the case $\rho_0 \to \rho_l$, the effectiveness curve of the buoyant air curtain approaches the effectiveness curve of the isothermal air curtain so that $\Lambda_\star \to \Lambda$. For our experimental range of L_j/h_b values, the effectiveness curve of the heated air curtain deviates at most by the factor of 1/2 from the experimentally measured curve of the isothermal air curtain, cf. Fig. 3. Thus, in our experiments we have

$$\frac{1}{2} \leq \frac{E\big|_{buoyant}}{E\big|_{isothermal}} \leq 1 \tag{16}$$

which leads to

$$1 \leq \frac{q_a\big|_{buoyant}}{q_a\big|_{isothermal}} \leq \frac{q}{2q_a\big|_{isothermal}} + \frac{1}{2} \tag{17}$$

so that

$$\frac{\Lambda - \Lambda_\star}{\Lambda_\star} \leq \frac{q}{2q_a\big|_{isothermal}} - \frac{1}{2} \leq 5 \tag{18}$$

where the last estimate arises if we assume that the maximum effectiveness for an isothermal air curtain is about $E \approx 0.9$ (Fig. 3) which is equivalent to $q/q_a\big|_{isothermal} \approx 10$.

In Fig. 6 we plot the measured data for the lower bound $\Lambda_\star$ to the energy efficiency Λ for our series of experiments. These points are superimposed with the data for the apparent effectiveness $E_\star$. Thereby, circles indicate the experimental runs in which $E_\star < 1$ (room is colder at the end of the experiment) and squares depict the cases $E_\star > 1$ (room is warmer at the end of the experiment). Red triangles show the experimental runs for which we calculated $\Lambda_\star > 1$. Since $\Lambda_\star$ is a lower bound for Λ, we conclude that for these experimental runs it was less energy efficient to use a buoyant air curtain compared with an isothermal air curtain. Blue diamonds show the experimental runs for which $\Lambda_\star < 1$ and it appears that here it is more energy efficient to use a buoyant air curtain. However, this notion might be misleading due to two reasons: first, $\Lambda_\star$ is just a lower bound and the actual value of Λ might be larger than 1 and, second, all blue diamonds are placed inside the circles corresponding to $E_\star < 1$. This means, that at the end of the experiment the room is cooler than at the beginning and it must be additionally heated until it reaches the initial room temperature T_l. This additional amount of heat load necessary to heat up the enclosure is not included into the definition of Λ.

The crucial observation here is that all the squares ($E_\star > 1$) and even some of the circles ($E_\star < 1$) contain red triangles which means $\Lambda \geq \Lambda_\star > 1$. We can interpolate the data and claim that also for the boundary case $E_\star = 1$ we should expect the energy efficiency Λ to be larger than 1. As a consequence, we can now draw an important conclusion: the use of a buoyant air curtain for which $E_\star = 1$ is equally or even less energy efficient than the use of an isothermal air curtain operating at room temperature. In summary, from the energetic point of view a buoyant air curtain has no advantages compared to an isothermal air curtain.

Note, in particular, that as previously mentioned, the definition of Λ in Eq. (14) does not contain the energy needed to heat up the room if the temperature inside decreases at the end of the experiment with the buoyant air curtain. Thus, we can obtain some points in Fig. 6 for which the buoyant air curtain is seemingly more energy efficient than a non-heated air curtain. We can expand Eq. (14) by defining

$$\tilde{\Lambda} = \frac{q_0\big|_{buoyant}(\rho_l - \rho_0) + \frac{V}{t}\left(\rho_l^{new}\big|_{buoyant} - \rho_l\right) + P}{q_a\big|_{isothermal}(\rho_d - \rho_l)} \tag{19}$$

where

$$\frac{V}{t}\left(\rho_l^{new} - \rho_l\right) = (\rho_d - \rho_l)\, q_a\big|_{buoyant} + (\rho_0 - \rho_l)\, \epsilon q_0\big|_{buoyant} \tag{20}$$

denotes the energy rate additionally needed to heat up the room and P is the energy consumption needed for operation of the ACD. P depends on the actual air curtain installation and, for example, in our experiments, P contains a term accounting for the energy consumption during the starting-up time of the ACD. The second term in Eq. (19) which accounts for additional heating of the room is only meaningful if the temperature inside the enclosure decreases. Thus, we use Eq. (19) if $E_\star < 1$ and Eq. (14) if $E_\star \geq 1$. We plot (the lower bound on) this modified energy efficiency in Fig. 7. We observe that once the energy needed for heating of the room is included, the modified energy efficiency is almost always larger than 1. The one experimental point for which it seems to be less than 1 can be attributed to a measurement error since in this case $\Lambda \approx 0.9$. This corroborates our claim that a heated air curtain is less energy efficient than an isothermal air curtain.

However, one should keep in mind that the presented results are inherent to one air curtain installation and

should not be conceived as absolute values for each possible air curtain installation. Thus, for different air curtain installations (e.g., with different initial inclination angles, initial turbulence levels or different geometries like return grill or double jets), the energy efficiency Λ on the $E_\star = 1$ curve might be a little less or larger than 1 so that either the isothermal or the buoyant regime might be slightly more energy efficient for different air curtain installations. A similar study as presented here is required for each special case to decide on the values of Λ on the $E_\star = 1$ curve, which are, however, not expected to differ significantly from 1.

5. Theoretical desrciption

Once a downwards blowing air curtain is heated it can be considered as a turbulent line source fountain which is subjected to a lateral pressure difference. The buoyancy force acting on the air curtain has hitherto been neglected in the theoretical description of the air curtain dynamics. Here, we propose a model for the behaviour of a buoyant air curtain.

5.1. Equations governing the dynamics of a buoyant air curtain

In the following, we assume that the air curtain is a Boussinesq fountain and possesses top-hat profiles of density and velocity. Furthermore, we use the entrainment model (cf. [17]) that the entrainment velocity into the air curtain is proportional to the centreline velocity in the fountain. Then, we can write down a system of partial differential equation governing the air curtain dynamics:

$$\begin{aligned}
&\frac{d}{dz}\left(bu\right) = \alpha_E u\sqrt{1+\tan^2\alpha}\\
&\frac{d}{dz}\left(bu^2\sin\alpha\right) = -g'\left(z-\frac{h_b}{2}\right)\\
&\frac{d}{dz}\left(bu^2\cos\alpha\right) = g'\left(z-\frac{h_b}{2}\right)\tan\alpha - \frac{bg}{\cos\alpha}\left(\frac{\rho_l}{\rho}-1\right)\\
&\frac{d}{dz}\left(bug\left(\frac{\rho_l}{\rho}-1\right)\right) = 0. \qquad (21)
\end{aligned}$$

We denote by u the centreline velocity and by b the width of the fountain perpendicular to the flow direction with u_0 and b_0 being the discharge velocity and the nozzle width. The inclination angle α of the fountain is measured from the vertical: α is defined as positive if the air curtain is inclined towards the dense fluid side of the doorway and negative otherwise. Recall that $g' = g\left(1-\gamma\right)$ and we introduce the notation $\triangle = g\left(\rho_l/\rho - 1\right)$ where ρ is the averaged fountain density at a certain height. At the nozzle, we have $\triangle_0 = g\left(\rho_l/\rho_0 - 1\right)$. The coordinate direction z is pointing vertically downwards, cf., Fig. 8.

The first equation in Eq. (21) describes the volume conservation. We assume that $\alpha_E u$ is the entrainment velocity into the line source fountain with α_E being the entrainment constant. Since the jet is inclined due to the transversal stack pressure acting on it, the entrainment into the fountain occurs not along the variation in the vertical direction dz but rather along the variation in the streamline coordinate ds. We can express $ds = \sqrt{dz^2+dx^2} = dz\sqrt{1+\tan^2\alpha}$, which explains the presence of the last factor in the volume conservation equation. Furthermore we define the flow rate through the fountain per unit length, i. e., door width, as $q = bu$. The initial condition for this flow rate is $q(0) = q_0/w_b$, where q_0 denotes the *total* initial flow rate through the air curtain device as has been used until now.

The second equation in Eq. (21) is the momentum flux conservation in the x - direction. We denote by $m = bu^2$ the momentum flux of the line fountain per unit length. Furthermore, we can define $m_x = bu^2\sin\alpha$ and $m_z = bu^2\cos\alpha$ as the x - and z - momentum fluxes per unit length, respectively. The x - momentum flux increases above the height $h_b/2$ since the air curtain is gradually deflected outwards due to the stack effect, and then it again starts to decrease below the height $h_b/2$ since now the forces acting on it due to the stack effect are reversed. The initial condition for the air curtain discharging vertically downwards is $m_x(0) = 0$.

The third equation in Eq. (21) describes the conservation of the momentum flux into the z - direction. The change in the z - momentum involves two contributions: first, the z - momentum undergoes changes due to the stack effect forces acting on the jet along varition dx, cf., Fig. 8. Thereby, dx can be expressed as $dx = dz\tan\alpha$. The second contribution to the z - momentum change arises due to the buoyancy force acting on the fountain. The air curtain divides the regions of fluids with density ρ_l and ρ_d. As an idealisation we can assume that the fountain is subjected to the buoyancy force $g\left(\rho_l - \rho\right)$, since for the cases considered here and relevant in practice we have $\rho_l - \rho_0 \gg \rho_d - \rho_l$. Thus, the total opposing buoyancy force acting on the air curtain in the control volume shown in Fig. 8 can be expressed as $b\triangle/\cos\alpha = bg\left(\rho_l/\rho - 1\right)/\cos\alpha$. The initial condition for the z-momentum flux if the air curtain discharged vertically downwards is $m_z(0) = m_0 = b_0u_0^2$.

The last equation in Eq. (21) is the conservation of the buoyancy flux per unit length. If we consider just

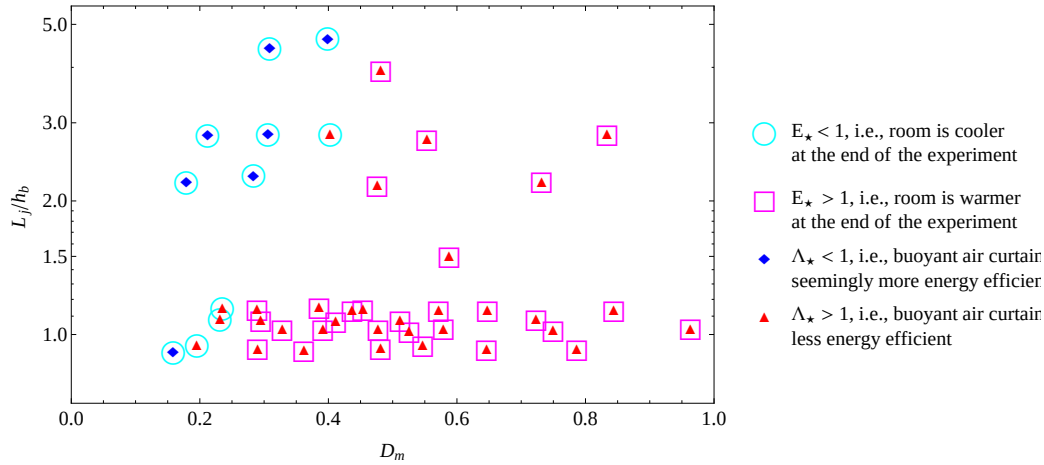

Figure 6: Experimentally measured data for the lower bound $\Lambda_\star$ of the energy efficiency Λ superimposed with measured data for the apparent effectiveness $E_\star$.

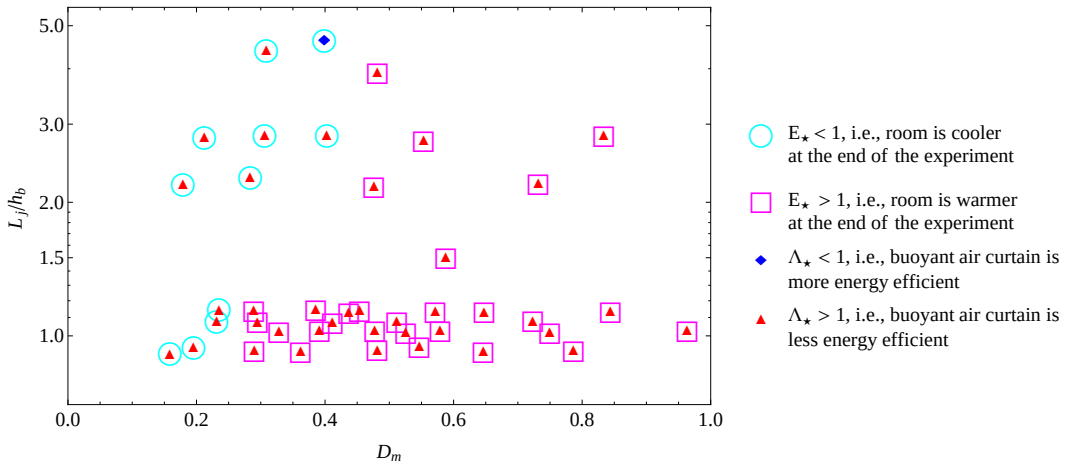

Figure 7: Experimentally measured data for the lower bound on the modified energy efficiency using Eq. (19) and Eq. (14) superimposed with measured data for the apparent effectiveness $E_\star$.

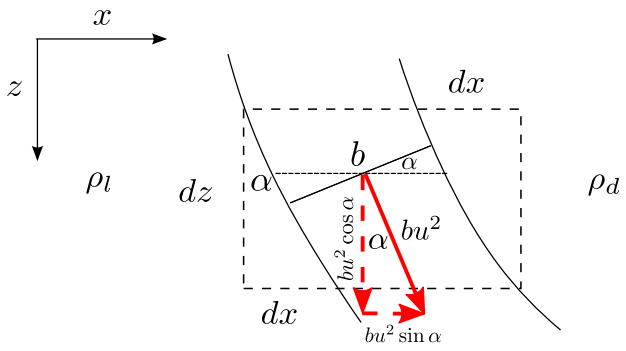

Figure 8: Configuration control volume.

one half of the fountain with width $b/2$ which is surrounded by the ambient fluid of density ρ_l then its buoyancy flux $bug\,(\rho_l/\rho - 1)$ is conserved. The initial condition is $q\triangle(0) = b_0 u_0 \triangle_0$.

Moreover, we have the following relations: $u = m/q = \sqrt{m_x^2 + m_z^2}/q$, $b = q^2/m = q^2/\sqrt{m_x^2 + m_z^2}$, $\cos\alpha = m_z/\sqrt{m_x^2 + m_z^2}$ and $\tan\alpha = m_x/m_z$.

With these definitions we can rewrite the above system of differential equations as:

$$\begin{aligned}
\frac{d}{dz}(q) &= \frac{\alpha_E}{m_z}\frac{m_x^2 + m_z^2}{q} \\
\frac{d}{dz}(m_x) &= -g'\left(z - \frac{h_b}{2}\right) \\
\frac{d}{dz}(m_z) &= +g'\left(z - \frac{h_b}{2}\right)\frac{m_x}{m_z} - \frac{q^2\triangle}{m_z} \\
\frac{d}{dz}(q\triangle) &= 0
\end{aligned} \tag{22}$$

with initial conditions

$$\begin{aligned}
q(0) &= q_0/w_b \\
m_x(0) &= 0 \\
m_z(0) &= b_0 u_0^2 \\
\triangle(0) &= g\,(\rho_l/\rho_0 - 1)
\end{aligned} \tag{23}$$

On the one hand, if there is no stack pressure difference across the doorway, the system Eq. (22) reduces to the well known equations for the line source fountain (cf. [18, 19]). On the other hand, if the air curtain is neutrally buoyant, we recover the usual momentum flux conservation equations of the air curtain (cf. [2]). Note, in particular, that the buoyancy force acting on the air curtain is calculated in terms of the light fluid density ρ_l.

5.2. Discussion of numerical solution and comparison to experiments

We solved the system Eq. (22) supplemented by boundary conditions Eq. (23) numerically. We set the entrainment parameter $\alpha_E = 0.22$ (see [20]). Note that we denote by b the whole width of the jet whereas Baines et al. [20] choose b as the half width. Therefore, in our case α_E should be twice the entrainment constant 0.106 used by Baines et al. in [20]. The air curtain breaks through if for some $z < h_b$ the z - momentum flux vanishes, i.e., we have $m_z = 0$. Otherwise, the air curtain is stable and impinges on the bottom of the doorway. Figure 9 shows the numerically calculated stability region of the buoyant air curtain for a range of parameters D_m and L_j.

We recognise that with decreasing L_j the minimum deflection modulus $D_{m,min}$ necessary for the stable air curtain rises from the value of 0.125 to approximately 0.2. This is consistent with the intuitive expectation that the initial momentum flux for the buoyant air curtain should be higher to overcome the additional buoyancy force acting on it. However, the increase in $D_{m,min}$ is marginal, and considering that for a real air curtain installation a safety factor should always be applied, this increase is unlikely to have any noticeable consequences.

The more remarkable observation is that below a certain normalised jet length L_j/h_b the air curtain ceases to be stable altogether. From Fig. 9 it can be recognised that the fountain behaviour dominates the air curtain if $L_j/h_b \lessapprox 0.8$ so that below this value the air curtain does not impinge on the bottom regardless of the deflection modulus value. However, the differential system Eq. (22) is suitable to calculate just the initial vertical extent of the fountain. Once the fountain reaches its initial penetration depth, the flow is reversed and the fountain core is surrounded by the upwards flow. The vertical extent of the fountain reduces and eventually the fountain fluctuates about a penetration depth which is smaller than the initial vertical extent. Burridge and Hunt [21] find experimentally that the ratio between the initial and the steady-state rise height of the (circular) fountain is approximately 1.34. If we apply this relationship to our case, we can argue that the air curtain is always unstable if $L_j/h_b \lessapprox 1.15$. This is in very good agreement with our experimental results. From Fig. 3 we observe a noticeable decrease in the effectiveness if $L_j/h_b \lessapprox 1.14$.

6. Discussion and application to real buildings

In this section we discuss in which way our experimental and numerical results are applicable to real

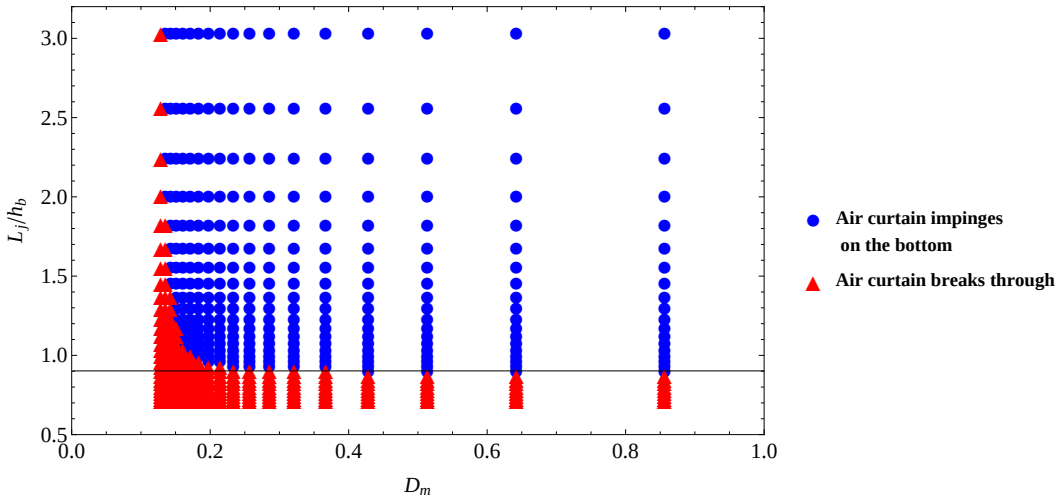

Figure 9: Numerically calculated stability region of the buoyant air curtain.

buildings and real air curtain installations.

In the previous section, we determined numerically that the minimum deflection modulus slightly rises from the value of $D_{m,min} \approx 0.125$ for a neutrally buoyant air curtain with $\rho_0 = \rho_l$ to the value of $D_{m,min} \approx 0.2$ before the fountain behaviour of the air curtain becomes dominant, cf. Fig. 9. However, in our model we neglect the build-up of the auxiliary pressure in the enclosure as discussed in [2, 5]. Hayes and Stoecker [5] predicted that this auxiliary pressure modifies the minimum deflection modulus so that $D_{m,min} \approx 0.15$. Thus, the correction for the additional buoyancy force is in the same order of magnitude as the correction for the auxiliary pressure. For a real air curtain installation a safety factor to the minimum deflection modulus should be applied in order to account for disturbances such as possible leakage around the air curtain edges, passage of people or vehicles, temperature and wind fluctuations. Thus, a real air curtain can be expected to become stable only if $D_m \approx 0.2$ if we choose the recommended safety factor ≈ 1.5. Therefore, for a real air curtain the increase in $D_{m,min}$ due to the additional buoyancy force is unlikely to have any noticeable consequences.

Let us now consider the result that below a certain value of L_j/h_b the fountain behaviour dominates and the air curtain does not reach the bottom. We argued in the previous section that theoretically we can expect air curtain instability below $L_j/h_b \lessapprox 1.15$ Also, our small-scale experiments suggest that the air curtain effectiveness starts to decrease noticeably if $L_j/h_b \lessapprox 1.15$.

For an air curtain installation with primarily human traffic such as found in doorways of shops and hotels, the discharge velocity is usually in the range 5 - 10 m/s, since higher velocities would be uncomfortable for people passing through. The width b_0 of the discharge nozzle usually varies between a few mm to a few cm depending on the actual installation site. Let us assume that the air cutain discharge with $u_0 = 6$ m/s from a nozzle of width $b_0 = 0.02$ cm. We choose the temperature inside the enclosure to be $T_l = 293$ K and the temperature outside to be $T_d = 278$ K. The primary air flow through the air curtain is assumed to be $T_0 = 313$ K. If we assume that the doorheight is about $h_b = 2.5$ m which is reasonable for a typical shop entrance doorway, then we have:

$$D_m \approx 0.2 \tag{24}$$

and

$$\frac{L_j}{h_b} \approx 1.54 \tag{25}$$

According to our experimental results, $L_j/h_b \approx 1.54$ should still be in the range in which the buoyancy does not have any perceptible effects on the air curtain effectiveness. However, increasing the discharge temperature of the air curtain by a further $10K$ to $T_0 = 323K$, which is still in the range used for real air curtain installations, yields:

$$\frac{L_j}{h_b} \approx 1.18 \tag{26}$$

Thus, for this choice of parameters the fountain behaviour of the heated air curtain becomes dominant and

in view of our experimental results this should have negative consequences on the sealing behaviour of the air curtain. According to our experimental results the air curtain effectiveness is reduced by 15-20% if $L_j/h_b \approx 1.15$. Therefore, if the air curtain is heated care must be exercised to keep the value of L_j/h_b high enough so that the effectiveness is not compromised.

Regarding the energy efficiency of the air curtain we could not find any evidence that a heated air curtain has any advantages compared to a non-heated air curtain. On the contrary, our experimental results indicate that a neutrally buoyant air curtain would be more energy efficient in most cases. However, each air curtain installation is different so that our results might not be universally applicable. For an actual air curtain installation different factors might influence the energy efficiency, such as the initial discharge angle of the air curtain or re-use of heated air by means of a return grill on the bottom of the doorway.

In practice, various reasons can make either the use of a non-heated or of a heated air curtain more preferable. If the air curtain should primarily form a particle barrier in order to prevent the transport of pollutants, insects or dust, then an isothermal air curtain should be favoured since its effectiveness is higher compared to the buoyant one. In contrast, a buoyant air curtain prevents the propagation of cold air along the bottom of the space which can constitute an unpleasant draught for occupants. Furthermore, a heated air curtain can assist in heating of the building and provide a better thermal comfort for people passing through on a cold winter day.

7. Conclusions

We studied the effects of an additional opposing buoyancy force on the dynamics and the sealing behaviour of a downwards blowing air curtain.

Our experimental results obtained using small-scale experiments with water as the working fluid indicate that the effectiveness of the air curtain starts to decrease if $L_j/h_b \lessapprox 1.15$. A similar limit on the stability of the air curtain was obtained when solving numerically a differential equation system which describes the air curtain dynamics. Our discussion of real air curtain installations shows that the value $L_j/h_b \approx 1.15$ is easily achievable in practice if the air curtain is heated. Therefore, caution must be excercised when using a heated air curtain so that the buoyancy force does not affect the air curtain sealing effectiveness.

Based on our experimental results we also discussed the energy efficiency of a heated air curtain versus a neutrally buoyant air curtain. Our experimental results showed that a heated air curtain is not likely to be more energy efficient than a non-heated air curtain.

This research has been supported by the EPSRC and Studienstiftung der Deutschen Volkes. We would like to thank D. Page-Croft for the technical support with the experimental setup.

[1] K. Sirén, Technical dimensioning of a vertically upwards blowing air curtain - part i, Energy and Buildings 35 (2003) 681–695.

[2] F. C. Hayes, W. F. Stoecker, Heat transfer characteristics of the air curtain, Transactions of the ASHRAE 75 (2) (1969) 153–167.

[3] K. Sirén, Technical dimensioning of a vertically upwards blowing air curtain - part ii, Energy and Buildings 35 (2003) 697–705.

[4] A. M. Foster, Computational Fluid Dynamics in Food Processing, CRC Press, Taylor & Francis Group, 2007, Ch. Chapter 7: CFD optimization of air movement through doorways in refrigerated rooms, pp. 167–194.

[5] F. C. Hayes, W. F. Stoecker, Design data for air curtains, Transactions of the ASHRAE 75 (1969) 168–180.

[6] R. H. Howell, M. Shibata, Optimum heat transfer through turbulent recirculated plane air curtains, Transactions of the ASHRAE 2567 (1980) 188–200.

[7] A. M. Foster, M. J. Swain, R. Barrett, P. D. D'Agaro, S. J. James, Effectiveness and optimum jet velocity for a plane jet air curtain used to restrict cold room infiltration, International Journal of Refrigeration 29 (2006) 692–699.

[8] L. Guyonnaud, C. Solliec, M. D. de Virel, C. Rey, Design of air curtains used for air confinement in tunnels, Experiments in Fluids 28 (2000) 377–384.

[9] A. M. Foster, M. J. Swain, R. Barrett, P. D. D'Agaro, L. P. Ketteringham, S. J. James, Three-dimensional effects of an air curtain used to restrict cold room infiltration, Applied Mathematics Modelling 31 (2007) 1109–1123.

[10] J. J. Costa, L. A. Oliveira, M. C. G. Silva, Energy savings by aerodynamic sealing with a downward-blowing plane air curtain - a numerical approach, Energy and Buildings 38 (2006) 1182–1193.

[11] J. C. Gonçalves, J. J. Costa, A. R. Figueiredo, A. M. G. Lopes, CFD modelling of aerodynamic sealing by vertical and horizontal air curtains, Energy and Buildings 52 (2012) 153–160.

[12] H. Giráldez, C. D. P. Segarra, I. Rodriguez, A. Oliva, Improved semi-analytical method for air curtains prediction, Energy and Buildings 66 (2013) 258–266.

[13] D. Frank, P. F. Linden, The effectiveness of an air curtain in the doorway of a ventilated building, Journal of Fluid Mechanics 756 (2014) 130–164.

[14] G. R. Hunt, C. J. Coffey, Characterising line fountains, Journal of Fluid Mechanics 623 (2009) 317–327.

[15] P. F. Linden, The fluid mechanics of natural ventilation, Annual Review of Fluid Mechanics 31 (1999) 201–238.

[16] D. J. Wilson, D. E. Kiel, Gravity driven counterflow through an open door in a sealed room, Building and Environment 25 (4) (1990) 379–388.

[17] B. R. Morton, G. Taylor, J. S. Turner, Turbulent Gravitational Convection from Maintained and Instantaneous Sources, Proceedings of the Royal Society of London. Series A. Mathematical and Physical Sciences 234 (1196) (1956) 1–23. doi:10.1098/rspa.1956.0011.

[18] T. S. van den Bremer, G. R. Hunt, Two-dimensional planar plumes: non-Boussinesq effects, Journal of Fluid Mechanics 750 (2014) 245–258. doi:10.1017/jfm.2014.252.

[19] T. S. van den Bremer, G. R. Hunt, Two-dimensional planar

plumes and fountains, Journal of Fluid Mechanics 750 (2014) 210–244. doi:10.1017/jfm.2014.246.

[20] W. D. Baines, J. S. Turner, I. H. Campbell, Turbulent fountains in an open chamber, Journal of Fluid Mechanics 212 (1990) 557–592.

[21] H. C. Burridge, G. R. Hunt, The rise heights of low- and high-froude-number turbulent axisymmetic fountains, Journal of Fluid Mechanics 691 (2012) 392–416.